Neutralization of slow multicharged ions at a clean gold surface: Electron-emission statistics

H. Kurz, F. Aumayr, C. Lemell, K. Töglhofer, and HP. Winter
Institut für Allgemeine Physik, Technische Universität Wien, Wiedner Hauptstraße 8-10/134, A-1040 Wien, Austria
(Received 1 February 1993)

Emission of slow electrons ($E_e \leq 60$ eV) induced by impact of slow multicharged ions (impact velocity $v_p \leq 2\times10^5$ m/s) onto an atomically clean, polycrystalline gold surface has been studied both experimentally and by numerical simulation, based on the resulting electron-emission statistics. The projectile ions (N^{q+}, $q=5,6$; Ne^{q+}, $q=5-10$; Ar^{q+}, $q=5-16$; Kr^{q+}, $q=5-10$; Xe^{q+}, $q=6,8,10$; I^{q+}, $q=16,20,23,25$) have been extracted from a recoil ion source pumped by the GSI UNILAC heavy-ion accelerator in Darmstadt, Germany. We discuss the shape of the experimentally obtained electron-emission statistics and, by means of numerical simulation based on the classical over-the-barrier model put forward recently by Burgdörfer, Lerner, and Meyer [Phys. Rev. A **44**, 5674 (1991)], identify the various processes contributing to the "above-surface" electron emission, i.e., taking place until projectile impact on the surface. In particular, for impact of slow ($E \geq 50$ eV) Ar^{12+} we show that most of the emitted electrons have energies below 50 eV, with the above-surface-produced fast Auger electrons being a small minority of less than 1%.

PACS number(s): 79.20.Nc, 31.50.+w, 79.90.+b

I. INTRODUCTION

In the past few years the interaction of highly charged ions with solid surfaces has become a topic of intense investigations at different laboratories [1–14]. In the preceding paper (paper I, Kurz *et al.* [15]) we have presented experimental data for total electron-emission yields resulting from the impact of slow multicharged ions (MCI's, typical projectile velocities between 2×10^4 and 2×10^5 m/s) as N^{q+} ($q=5,6$), Ne^{q+} ($q=5-10$), Ar^{q+} ($q=5-16$), Kr^{q+} ($q=5-10$), Xe^{q+} ($q=6,8,10$), and I^{q+} ($q=16,20,23,25$) on a clean polycrystalline gold surface. All measured yields were found first to gradually decrease with increasing impact velocity but then to level off towards an apparent velocity-independent contribution [6,15]. A systematic comparison between our experimental data and modeling calculations, which involved the classical over-the-barrier model (CBM) introduced by Burgdörfer, Lerner, and Meyer [11], indicated that at least three different mechanisms contribute to the experimentally observable total "above-surface" electron emission yields (cf. [15]), namely, (i) autoionization (AI) of the multiply excited "hollow atoms" formed due to fast resonance neutralization on the projectiles' way towards the surface; (ii) promotion above the vacuum barrier of electrons previously captured by the projectile, due to their combined action of self- and image-charge screening near the surface (SS+IS); and finally (iii) "peeling-off" (PO) of all electrons still bound in highly excited projectile states at the very moment of surface impact.

Our model calculations suggested that the latter two mechanisms (PO and SS+IS) are responsible for the contribution to the slow-electron yield which is emitted almost independent of the projectile's velocity, whereas the velocity-dependent part has to be attributed to AI. However, some estimates for the fraction of electrons emitted from the projectile and absorbed by the Au surface have been necessary to reach good agreement between the measured and calculated yields. The total sum of all three contributions [$\Sigma1=$(AI)+(PO)+(SS+IS)] clearly overestimated the measured yields, but no clear decision was possible between the following two assumptions, which both led to comparably good agreement with the experimental data.

(1) For $\Sigma1\times0.7$ it was assumed that 30% of all electrons emitted are reabsorbed by the solid.

(2) Under the model assumption $\Sigma2=$(PO)+(SS+SI)+0.5(AI) all electrons promoted or peeled off, but only 50% of those due to AI can leave the surface and reach the detector.

The results presented in Ref. [15] have been determined by means of an experimental technique that actually delivers the electron-emission statistics (ES), i.e., the probabilities W_n for emission of $n=1$, 2, etc., electrons per impinging MCI [6,15–17], with the yield γ being the first momentum of the ES.

$$\gamma=\sum_{n=1}^{\infty} nW_n, \quad \sum_{n=0}^{\infty} W_n=1 \ . \tag{1}$$

So far no use has been made of the information contained in the ES itself or in its other momenta (e.g., the standard deviation) of the measured statistical distributions, apart from the observation [6] that the measured distributions are generally narrower than a Poissonian distribution with the same mean value γ.

In this paper we first present experimentally determined ES distributions, in particular their evaluated standard deviations (Sec. II) and then show that these ES's are not only consistent with the picture developed in Ref. [15], but also deliver further useful information (Sec. IV). To this purpose we had to change our rate equation code used in Ref. [15] to a Monte Carlo program, as described in Sec. III.

II. PRESENTATION OF EXPERIMENTAL RESULTS

The statistical behavior of above-surface emission of slow electrons ($E_e \leq 60$ eV) caused by impact of multicharged ions with "nominal" impact velocities between 2×10^4 and 2×10^5 m/s (the influence of image charge attraction on impact velocities has been discussed, e.g., in Refs. [11,15]) onto an atomically clean, polycrystalline gold surface has been studied using various multicharged ions produced by a recoil-ion source at GSI Darmstadt [6,15]. The ES method and the data-evaluation procedures for determination of the ES have been described in detail in Refs. [6,15–17]. All measurements have been performed under UHV conditions (background pressure $\leq 3\times10^{-8}$ Pa), applying regular sputter cleaning of the Au target surface.

Figure 1 shows measured ES resulting from impact of Ar^{12+} ions (nominal impact energies of 50, 500, and 4800 eV, respectively) on clean polycrystalline gold. Gaussian distributions (dashed lines) fit the measured data quite well, whereas a Poissonian (solid line for the example of 500-eV Ar^{12+}) with the same mean value γ is clearly too broad. Obviously, with increasing projectile velocity not only the mean values γ of the probability distributions, but also their corresponding widths, i.e., the standard deviations σ as defined by

$$\sigma = \left[\sum_{n=0}^{\infty} (n-\gamma)^2 W_n \right]^{1/2} , \tag{2}$$

are decreasing. For a Poissonian distribution P_n,

$$P_n(\gamma) = \frac{\gamma^n}{n!} e^{-\gamma} , \tag{3}$$

the standard deviation σ is not a free parameter but related to the mean value γ by

$$\sigma = \sqrt{\gamma} . \tag{4}$$

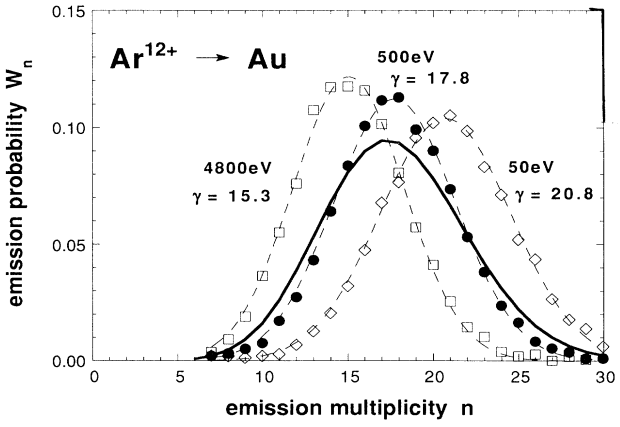

FIG. 1. Measured electron-emission statistics for impact of Ar^{12+} ions with different impact energies on clean polycrystalline gold. The dashed lines are fitted Gaussian distributions. The 500-eV data have also been compared to a Poissonian distribution (solid line) with the relevant mean value γ.

The results shown in Fig. 1 are typical for all projectile ion species investigated. With the exception of comparably low charge states (e.g., Ar^{5+}), Gaussian distributions can be fitted rather well to the measured emission probabilities W_n (with only minor asymmetries as noticeable in Fig. 1), whereas corresponding Poissonian distributions are in all cases clearly too broad.

As typical examples, standard deviations σ evaluated from measured probability distributions for impact of Ar^{q+} ($q = 8, 10, 12, 14, 16$) and Ne^{8+}, Ne^{10+}, I^{16+}, I^{20+} have been plotted in Figs. 2(a) and 2(b), respectively, versus projectile impact velocity. With increasing projectile velocity not only the total yields γ (cf. [15]), but also the standard deviations decrease.

For projectile charge states $q > 10$ the measured standard deviations show a remarkable behavior, as can be seen from Figs. 2(c) and 2(d). If a "reduced" standard deviation, i.e., σ divided by the square root of the corresponding total yield γ, is plotted versus impact velocity, all measured data nicely follow a "universal curve" independent of charge state, species, and even impact velocity. Considering Eq. (3) this simply means that our measured ES feature a standard deviation that amounts to about (85±5)% of that of a Poissonian distribution with the same mean value γ. However, for projectile charge states $q < 8$ (e.g., Ar^{5+}) deviations from this universal curve by up to 40% have been observed.

III. DISCUSSION OF EXPERIMENTAL RESULTS IN COMPARISON WITH MODEL CALCULATIONS

In order to model the statistical behavior of MCI-induced above-surface emission of slow electrons, we have applied the classical over-barrier model developed by Burgdörfer, Lerner, and Meyer [11]. A MCI (charge state q) approaching a metal surface (cf. Fig. 7 of paper I) at a critical distance $R_c(q)$ starts to capture electrons resonantly from the metal conduction band [resonant neutralization (RN) [18,19]] into highly excited projectile states. This critical distance is reached when the potential barrier, formed by the projectile's potential, its image potential, and the image potential of the electron to be captured, is decreased below the Fermi level of the metal [11]. RN stops as soon as the captured electrons decrease the ion charge state q and, as a consequence, the potential barrier again rises above the Fermi level. With further approach toward the surface, RN will continue and thus multiply excited hollow atoms will be produced (cf. discussion in [15]). In parallel to RN, Auger processes will lead to electron emission into vacuum (autoionization, AI) or empty states of the conduction band [Auger loss (AL) to the conduction band] [11]. Due to the combined action of the image charge of the ion core [image shift (IS)] and screening of the charge of the ion core by electrons already occupying lower levels due to preceding RN or AI processes [screening shift (SS)] the projectile energy levels are shifted upwards [11,14] (cf. Fig. 7 of paper I). Electrons promoted in this way above the potential barrier and the Fermi level can be lost again into empty states of the conduction band [resonant ionization

(RI)]. As described in more detail in paper I [15], in addition to AI two other electron-emission mechanisms had to be included in our model. On the one hand, electrons "surviving" AI and RI can be promoted above the vacuum level (IS+SS promotion) and thus escape (cf. Fig. 2). On the other hand, as soon as a hollow atom strikes the surface, its still-populated outer shells become peeled off because of dynamical screening inside the solid [11,20]. We have to assume that an electron becomes subject to PO if its Bohr radius at the moment of projectile impact on the surface is larger than the screening length for surface plasmons $\lambda_s = v_F/\omega_p$ of the metal (v_F is the Fermi velocity and ω_p is the surface plasmon frequency).

For comparison with measured electron yields, in Ref. [15] we have solved the set of coupled rate equations of the populations P_n of the nth shells of the projectile as a function of its distance from the surface [11], with the above-described assumptions. We thus could obtain the number of autoionized electrons, the number of electrons promoted into vacuum due to SS+IS, and the number of electrons subject to PO at the moment of surface impact, respectively (cf. Figs. 8–10 of Ref. [15]).

Since such a rate-equation approach is only adequate to describe the mean value γ but not the statistical distribution of emitted electrons, a Monte Carlo - code version of the CBM model has been developed. This was achieved by transforming the rates (AI, AL, RN, RI, etc.) used in Ref. [15] into probabilities and running a large number of individual projectile histories. As a typical result, in Fig. 3 we present histograms for the three individual electron-emission mechanisms (AI, SS+IS promotion, and PO) as calculated for impact of 3×10^4-m/s Ar^{12+} ions on Au. In contrast to AI, which leads to a relatively wide Gaussian-shaped probability distribution [Fig. 3(a)], the PO mechanism [Fig. 3(c)] involves a highly deterministic and asymmetric structure with the highest probability for emission of $n=12$ electrons (cf. Ref. [15]), whereas IS+SS promotion remains comparably unimportant. In combination, IS+SS and PO (which according to our findings in Ref. [15] are responsible for the nearly velocity-independent part of the total electron yield) result in an almost symmetric distribution, which—at the given impact velocity of 3×10^4 m/s for Ar^{12+} impact on Au—is by far narrower than the AI distribution, although it features about the same mean value as the AI-related distribution.

In order to compare the results of our model calculations to the measured emission statistics one cannot simply "add up" all three contributions as shown in Fig. 3, but has to take into account that a fraction of the electrons emitted from the projectile towards the surface may be absorbed by the latter, whereas other electrons will be

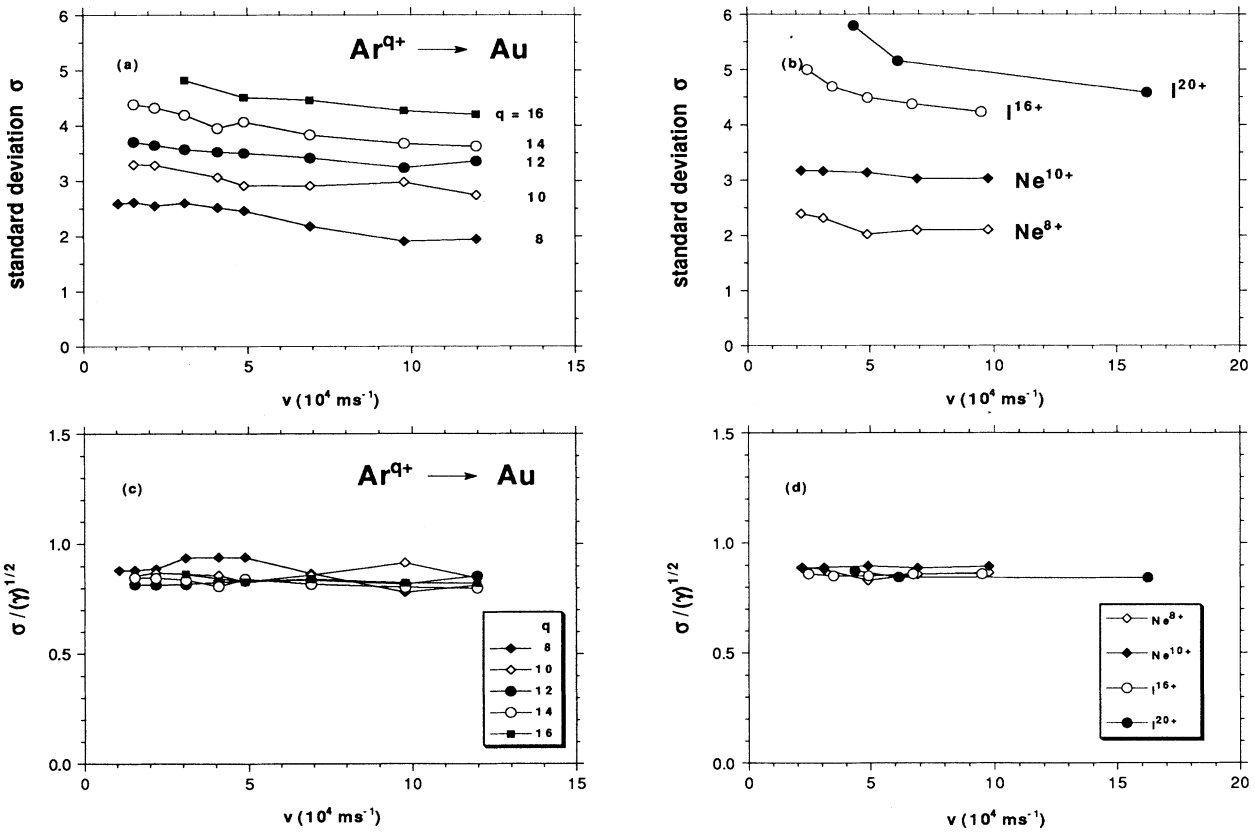

FIG. 2. Standard deviations σ evaluated from measured probability distributions for impact of (a) Ar^{q+} ($q=9,10,12,14,16$) and (b) Ne^{8+}, Ne^{10+}, I^{16+}, and I^{20+}, respectively, and (c), (d) corresponding "reduced" standard deviations (i.e., σ divided by the square root of the corresponding total yields γ) vs impact velocity; see text.

reflected from the metal surface, some of them also producing secondary electrons. Since, to our knowledge, there are no applicable data on reflection and secondary electron emission due to impact of primary electrons in the 1–5-eV energy range, we made alternatively three rather crude estimates ($\Sigma 1$, $\Sigma 2$, and $\Sigma 1 \times 0.7$, as described in Sec. I and already discussed in Ref. [15]).

In Fig. 4 the emission statistics measured for 3×10^4-m/s Ar^{12+} impact on Au has been compared under these three assumptions with results of our Monte Carlo calculations. As already mentioned in [15], $\Sigma 1$ clearly overestimates the number of detected electrons, while the agreement between the mean values from our measurements and the $\Sigma 1 \times 0.7$—as well as the $\Sigma 2$—model calculations are surprisingly good (in the particular case shown in Fig. 4, but not in general, a still better agreement with the experimental data could have been obtained by using a factor of 0.65 instead of 0.7). However, when considering the width of the calculated statistical distributions, the experimental standard deviation σ is far better reproduced by the $\Sigma 1 \times 0.7$-model calculations, whereas the $\Sigma 2$ distribution is obviously too narrow.

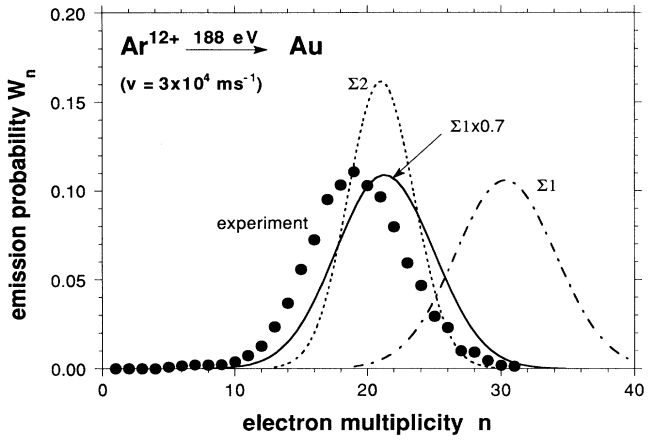

FIG. 4. Electron-emission statistics measured for 3×10^4-m/s Ar^{12+} impact on Au (symbols) compared to results of the Monte Carlo-model calculations (lines) derived under different assumptions for the reabsorbed fraction of emitted electrons (see text).

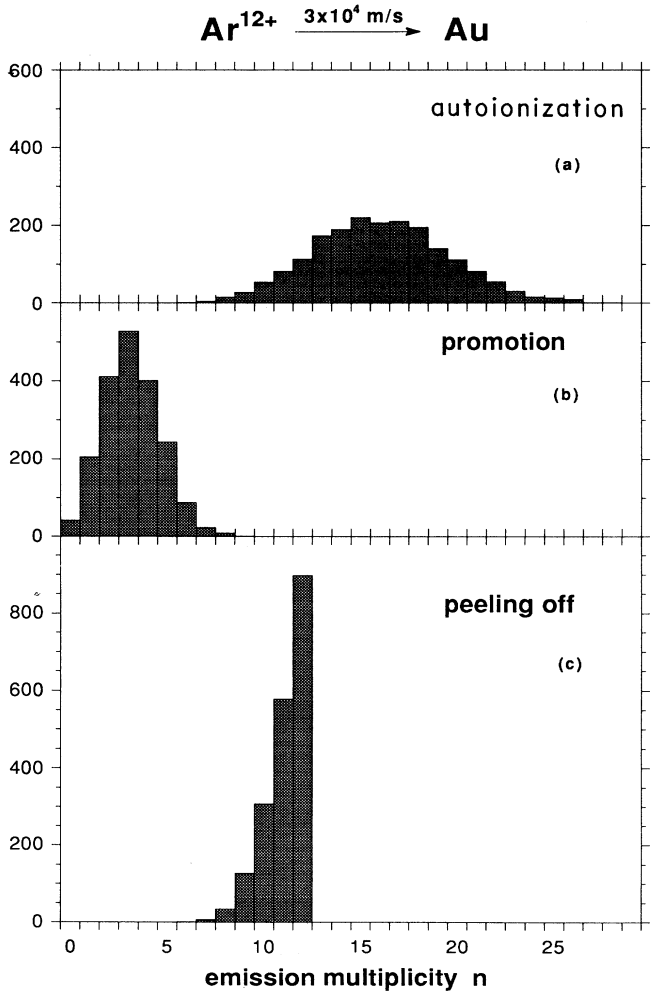

FIG. 3. Histograms for the three different electron-emission mechanisms. (a) Autoionization (AI), (b) screening and image-shift promotion (SS+IS), and (c) peeling off (PO), as calculated for impact of 2000 Ar^{12+} ions on Au (nominal impact velocity 3×10^4 m/s). AI causes a relatively broad Gaussian-shaped probability distribution, whereas the PO-related distribution features a highly deterministic and asymmetric structure.

This behavior was found to hold almost generally and irrespective of the impact velocity, as has been demonstrated in Fig. 5, where reduced standard deviations $\sigma/(\gamma)^{1/2}$ were plotted versus impact velocity for Ar^{12+} impact on Au. Satisfactory agreement with the experimental data points is only obtained under the assumption $\Sigma 1 \times 0.7$, with the calculated distributions for $\Sigma 2$ or $\Sigma 1$ being by far (up to 50%) too narrow. By comparing with our measured electron-emission statistics, we can thus definitely rule out the assumptions $\Sigma 2$ and $\Sigma 1$ and extract

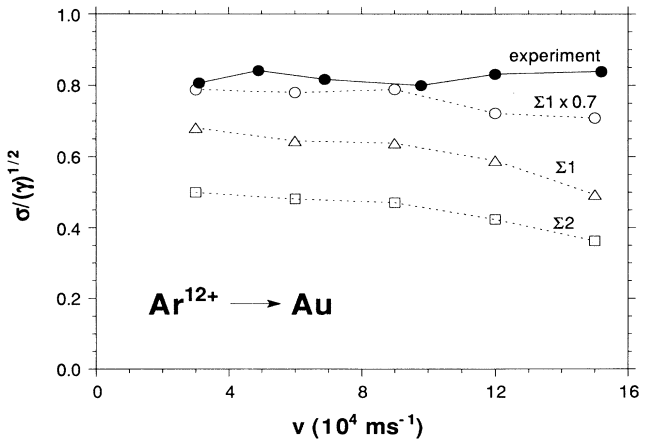

FIG. 5. Reduced standard deviations $\sigma/(\gamma)^{1/2}$ for Ar^{12+} impact on Au, vs impact velocity, as measured (solid circles) and calculated (open symbols) under different assumptions for the reabsorbed fraction of electrons, respectively (see text).

the reasonable information that roughly a fraction of $(30\pm10)\%$ of all emitted electrons is effectively absorbed by the solid, independent of the particular emission mechanism.

Finally, our Monte Carlo code has also been used to calculate the energy distribution of electrons emitted in the AI processes (the energies of electrons emitted due to PO and SS+IS probably remain below 20 eV). Results for 3×10^4-m/s Ar^{12+} impact on Au have been shown in Fig. 6. At around 200 eV we find some fast Auger electrons filling an Ar L-shell hole (*LMM*, *LMN* transitions, etc.) and electrons at around 100 eV can be attributed to M Auger transitions (*MNN* transitions, etc.). However, more than 99% of all AI electrons are emitted with energies of less than 50 eV, and 90% with less than 20 eV. Although our experiment was only designed to measure electrons with $E_e < 60$ eV (cf. [6,16]), such derived yields and ES distributions can thus be considered to agree almost completely with the total electron emission taking place in front of the surface.

We should remark, however, that after the projectiles have penetrated the surface barrier, their electronic configuration will be drastically changed [15]. Because of this, still present inner-shell vacancies can be rapidly filled via Auger electron transitions, giving rise to emission of much faster electrons (e.g., $E_e \approx 210$ eV for Ar *LMM* transitions [2]) than detectable by our setup.

Some of these fast Auger electrons may also produce slow "subsurface secondary electrons," which again will be detected by our setup but not be taken into account by our calculations. However, we estimate this possible subsurface secondary electrons to be much less abundant than the above-surface slow electrons discussed here, considering a secondary-electron emission coefficient of about 1 for 210-eV primary electrons impinging onto clean gold (cf. [21] and references therein) and some discrimination due to the creation of the primary electrons inside the solid.

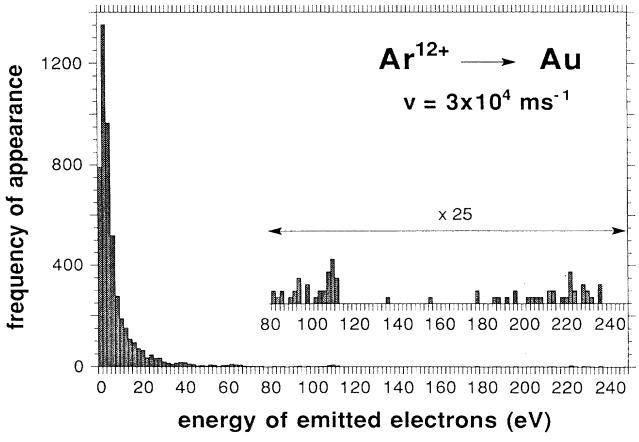

FIG. 6. Calculated energy distribution of electrons emitted via AI processes during the approach of Ar^{12+} (3×10^4 m/s) towards the Au surface. Fast Auger electrons filling the Ar L and Ar M shells appear at around 200 and 100 eV, respectively. More than 99% of all AI electrons emitted above the surface involve energies of less than 50 eV.

IV. SUMMARY AND CONCLUSIONS

Our recent discussion of the impact-velocity dependence of experimentally determined total electron yields [6,15] resulted in hints to the relative contributions by and nature of some principally different emission processes, which depend not only on the charge state of the primary MCI, but also on its structure, i.e., species. The present study shows that further details on these different emission processes, which are contributing to the total "above-the-surface" electron emission, can be obtained from the electron-emission statistics themselves, which in all cases is substantially narrower than a Poissonian distribution having the relevant total electron yield as mean value. A Poissonian shape has to be expected, however, if the observed, relatively large numbers of electrons were emitted in an appropriately large number of statistically independent, single events. From the systematics of our experimental results we thus could obtain new details on the formation and autoionization of the so-called hollow atoms, which are transiently formed during the approach of a slow MCI toward a metal surface. To support this still qualitative picture, Monte Carlo-model calculations based on the recently developed classical over-barrier approach of Burgdörfer, Lerner, and Meyer [11] have been performed and led to a very satisfactory, almost quantitative agreement with the experimental data. Roughly speaking, at least three sources for the above-surface slow-electron emission can be distinguished, viz., autoionization of the multiply excited hollow atoms on their way toward the surface; promotion above the vacuum barrier of electrons previously captured by the projectile, due to their self- and image-charge shielding near the surface; and, finally, peeling off of all electrons still bound in highly excited projectile states until the very moment of surface impact. Whereas the first mechanism correlates with a relatively broad emission statistics, the second and third produce considerably narrower distributions, causing the experimentally observable statistics as the convolution of the three partial processes to become considerably narrower than a Poissonian distribution with the same mean value. A non-negligible fraction (about 30%) of all electrons emitted by the oncoming projectile was assumed to be absorbed by the surface, to achieve proper agreement between our calculations and experimental results.

We especially point out that most of the electrons emitted from the hollow atoms above the surface have energies of less than 20 eV, whereas the much faster Auger electrons, which are produced due to inner-shell transitions, remain a small minority of typically less than 1% of the total emission yields. However, after the projectiles have entered the solid and their outer electrons have been peeled off, they should become rapidly repopulated into comparably much stronger bound shells (cf. [15]). This, in turn, will initiate predominant emission of fast electrons due to Auger transitions into the still largely empty inner shells, since the latter, due to lack of

sufficient time, have not yet been filled above the surface. Slow subsurface secondary electrons, which are possibly produced if these fast Auger electrons are ejected inside the solid, will be detected by our setup as well, but for the case of Ar^{12+} are believed to be much less abundant than the slow electrons emitted from the hollow Ar atom still above the surface. However, for lower charged projectiles that are forming in the course of their neutralization inner-shell vacancies (e.g., N^{6+} or Ne^{9+}), the fraction of subsurface secondary electrons might become relatively more important.

ACKNOWLEDGMENTS

The authors express their gratitude to Professor J. Burgdörfer for useful suggestions concerning his CBM model and to Dr. Rido Mann and other staff members of GSI Darmstadt, Germany, for their excellent help provided to the experimental part of this study. The latter has been supported by Austrian Fonds zur Förderung der wissenschaftlichen Forschung (Project No. P8315TEC) and by Kommission zur Koordination der Kernfusionsforschung at the Austrian Academy of Sciences.

[1] M. Delaunay, M. Fehringer, R. Geller, D. Hitz, P. Varga, and HP. Winter, Phys. Rev. B **35**, 4232 (1987).
[2] S. T. de Zwart, Ph.D. thesis, Rijksuniversiteit Groningen, 1987.
[3] D. M. Zehner, S. H. Overbury, C. C. Havener, F. W. Meyer, and W. Heiland, Surf. Sci. **178**, 359 (1986).
[4] F. W. Meyer, S. H. Overbury, C. C. Havener, P. A. Zeijlmans van Emmichoven, J. Burgdörfer, and D. M. Zehner, Phys. Rev. A **44**, 7214 (1991).
[5] F. W. Meyer, S. H. Overbury, C. C. Havener, P. A. Zeijlmans van Emmichoven, and D. M. Zehner, Phys. Rev. Lett. **67**, 723 (1991).
[6] H. Kurz, K. Töglhofer, HP. Winter, F. Aumayr, and R. Mann, Phys. Rev. Lett. **69**, 1140 (1992).
[7] J. W. McDonald, D. Schneider, M. W. Clark, and D. Dewitt, Phys. Rev. Lett. **68**, 2297 (1992).
[8] R. Köhrbrück, K. Sommer, J. P. Biersack, J. Bleck-Neuhaus, S. Schippers, P. Roncin, D. Lecler, F. Fremont, and N. Stolterfoht, Phys. Rev. A **45**, 4653 (1992).
[9] L. Folkerts and R. Morgenstern, Europhys. Lett. **13**, 377 (1990).
[10] L. Folkerts, Ph.D. thesis, Rijksuniversiteit Groningen, 1992.
[11] J. Burgdörfer, P. Lerner, and F. W. Meyer, Phys. Rev. A **44**, 5674 (1991).
[12] J. P. Briand, L. de Billy, P. Charles, S. Essabaa, P. Briand, R. Geller, J. P. Desclaux, S. Bliman, and C. Ristori, Phys. Rev. Lett. **65**, 159 (1990).
[13] J. N. Bardsley and B. M. Penetrante, Comments At. Mol. Phys. **27**, 43 (1991).
[14] H. J. Andrä, A. Simionovici, T. Lamy, A. Brenac, G. Lamboley, A. Pesnelle, S. Andriamonje, A. Fleury, M. Bonnefoy, M. Chassevent, and J. J. Bonnet, in *Electronic and Atomic Collisions,* edited by W. R. MacGillivray, I. E. McCarthy, and M. C. Standage (Hilger, Bristol, 1992), p. 89.
[15] H. Kurz, F. Aumayr, C. Lemell, K. Töglhofer, and HP. Winter, preceding paper, Phys. Rev. A **48**, 2182 (1993).
[16] G. Lakits, F. Aumayr, M. Heim, and HP. Winter, Phys. Rev. A **42**, 5780 (1990).
[17] F. Aumayr, G. Lakits, and HP. Winter, Appl. Surf. Sci. **47**, 139 (1991).
[18] H. D. Hagstrum, Phys. Rev. **96**, 325, 336 (1954).
[19] U. Wille, Surf. Sci. Lett. **280**, L291 (1993).
[20] J. Müller and J. Burgdörfer, Phys. Rev. A **43**, 6027 (1991).
[21] E. W. Thomas, in *Atomic and Plasma Material Interaction Data for Fusion,* edited by R. K. Janev, Nucl. Fusion Suppl. (IAEA, Vienna, 1991), Vol. 1.